Generation of vacuum-ultraviolet radiation in H_2 by nonlinear optical processes near the *EF*- and *B*-state resonances

U. Czarnetzki and H. F. Döbele
Institut für Laser-und Plasmaphysik, Universität Gesamthochschule Essen, D-4300 Essen 1, Federal Republic of Germany
(Received 17 June 1991)

We report on the observation of several nonlinear optical processes in connection with two-photon excitation of H_2 by 193-nm radiation generated by a narrow-bandwidth ArF laser system: stimulated electronic hyper-Raman scattering, parametric four-wave mixing (PFWM), and stimulated resonant Raman scattering (SRRS). These processes lead to the generation of several intense lines in the ir and vacuum ultraviolet (vuv). vuv generation occurs by two interconnected schemes: first, a vuv wave at $\lambda \sim 109$ nm is generated by PFWM (power up to 16 kW). This wave subsequently generates Stokes lines around $\lambda \sim 150$ nm by SRRS. The frequencies of these waves are tunable over spectral intervals of ~ 20 cm^{-1} by phase matching with admixture of various gases (e.g., noble gases, N_2, D_2). With additional irradiation of ir laser radiation, four-wave mixing (FWM) takes place. In this case, continuously tunable vuv radiation (tuning range ~ 600 cm^{-1}) can be generated with power in the 10- and 100-kW range. The tuning ranges are localized around the rovibronic resonances *X-B*. FWM is not possible on resonance. As in the case of PFWM, Stokes lines are generated by SRRS, tunable over intervals up to ~ 60 cm^{-1}. The susceptibilities governing the processes involved are calculated. The agreement between the theoretical expectations and the experimental results is very good with respect to the frequency dependence. The calculated absolute values of the vuv intensities, however, turn out to be by far too high. This is due to the neglect of several limiting processes which will be discussed together with the experimental results. In addition to the processes mentioned above, several *B-X* resonance transitions exhibit a limited tunability (~ 10 cm^{-1}). It is proposed to explain this tunability in terms of stimulated two-photon emission.

PACS number(s): 42.65.Ky, 33.80.Rv, 42.65.Dr

I. INTRODUCTION

Methods of nonlinear optics like difference and sum-frequency mixing or frequency tripling in gases and vapors have been successfully applied to the generation of coherent vacuum-ultraviolet (vuv) radiation since the 1970s. Metal vapors as well as noble gases were found to have excellent characteristics as nonlinear media [1–4]. Molecular hydrogen, however, was mainly used in connection with stimulated Raman scattering (SRS), whereby generation of tunable radiation down to $\lambda = 116$ nm by high-order anti-Stokes scattering has been reported [5]. With the potential of the ArF laser to generate high-power, tunable narrow-bandwidth radiation around $\lambda = 193$ nm, two-photon excitation of ground-state $H_2(X\,^1\Sigma_g^+)$ into the $EF\,^1\Sigma_g^+$ state was realized several years ago [6–11]. The two-photon absorption cross section turned out to be large enough to allow a substantial inversion to be built up in several rovibronic levels of the *EF* state with respect to the energetically lower $B\,^1\Sigma_u^+$ state [Fig. 1(a)]. This leads to amplified spontaneous emission (ASE) in the near ir (750–920 nm). Due to this radiation process, *B*-state levels are populated and a population inversion relative to higher rovibronic levels of the electronic ground state is created. Strong ASE radiation in the so-called Lyman band is subsequently observed. This radiation is in the vuv spectral range ($\lambda = 130$–160 nm). It was also shown that, taking advantage of this two-photon resonance in H_2, radiation in the spectral range around 79 nm can be generated by sum-frequency mixing [12].

We have communicated in an earlier paper that in case of two-photon excitation of H_2 in parallel to the ASE radiation, a tunable Stokes component in the transition *EF-B* develops due to stimulated electronic hyper-Raman scattering (SEHRS) [10] [Fig. 1(b)]. Besides these ASE and SEHRS lines, additional lines were observed in the near ir that do not match the energy level scheme of H_2. These additional lines are redshifted with respect to the known transitions and are tunable with variation of the frequency of the exciting uv source. Correlated with these lines we find corresponding lines in the vuv which are spectrally blueshifted by the same amount with respect to the Lyman lines. It was further found that with additional irradiation in the ir strong vuv lines are generated which terminate on para-H_2 (p-H_2) ground-state levels, whereas the two-photon excitation by the uv laser takes place at ortho-H_2 (o-H_2) (and vice versa) [11].

We will show in the following that the phenomena observed are due to the combined action of parametric four-wave mixing (PFWM) or—with irradiation of additional radiation in the ir—of four-wave mixing (FWM) and stimulated resonant Raman scattering (SRRS) [13] [Figs. 1(c) and 1(d)]. To our knowledge, comparable effects have been observed only in Na vapor at substantially longer wavelengths [14].

In the case of parametric four-wave mixing, two photons of the uv pump laser decay into an ir and a vuv photon [Fig. 1(c)], similarly to the three-photon process in crystals [called optical parametric fluorescence (OPF)

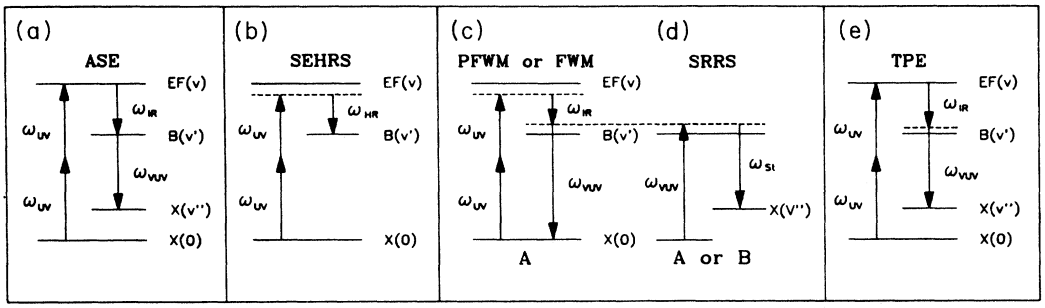

FIG. 1. Simplified energy-level diagram explaining the nonlinear processes (to simplify the situation no rotational levels are indicated): (a) Amplified spontaneous emission (ASE) at fixed frequencies in the IR (*EF-B*) and the vuv (*B-X*) subsequent to resonant two-photon excitation with ω_{uv}. (b) Stimulated electronic hyper-Raman scattering (SEHRS) leading to tunable ir radiation at ω_{HR}. (c) Parametric four-wave mixing (PFWM) generating tunable ir and vuv radiation. With additional irradiation of ir radiation tunable vuv radiation is generated by four-wave mixing (FWM). (d) Stimulated resonant Raman scattering of vuv radiation generated by PFWM or FWM with Stokes radiation ω_{st} in the near vuv. While PFWM or FWM takes place in molecules of type A (e.g., *o*-H_2) the subsequent SRRS occurs in type A or in type B molecules (e.g.,*p*-H_2 or D_2). (e) Stimulated two-photon emission (TPE) subsequent to resonance two-photon excitation and additional irradiation of ω_{ir}. A tunable output at ω_{vuv} is generated.

[15]]. The frequencies of the ir and vuv waves are determined by the phase-matching condition $\Delta k = 0$. The ir lines were observed in our earlier experiments as the redshifted satellites mentioned above, whereas the related vuv lines, being fundamental for the understanding of the process, could not be detected due to the short wavelength (108–111 nm) where the transmission of the optical components used was insufficient. In order to satisfy the phase-matching condition, anomalous dispersion at the frequency of the vuv line is required. This condition can be fulfilled with the frequency slightly exceeding the resonance frequency of a *X-B* transition. The vuv wave of frequency close to a *X-B* resonance exhibits a very large Raman cross section. In contrast to common SRS where we have the selection rule $\Delta v = \pm 1$, the Stokes transitions in a quasiresonant situation are governed by the Franck-Condon coefficients (FCC) for a transition of the intermediate Raman level back to rovibronic levels of the electronic ground state. We observed these Stokes components as blueshifted satellites in the Lyman band in our earlier experiments [11]. The ir radiation generated by PFWM and Stokes radiation generated by SRRS of the PFWM vuv wave have the same properties as if they "use" a common level in the range of the *B* states [Figs. 1(c) and 1(d)]. This puzzling behavior misguided us to the hypothesis that the *B*-state levels might be shifted due to the formation of collisional complexes [11].

Irradiation of additional ir laser radiation allows very efficient four-wave mixing with almost continuous tuning ranges of ~ 600 cm^{-1} around the various vibrational *B*-state levels. Ortho-para transitions result from SRRS at *p*-H_2 subsequent to the generation of a vuv wave by FWM in *o*-H_2 [Figs. 1(c) and 1(d)]. The related Stokes radiation is also tunable. The tuning range is considerably narrower (20–60 cm^{-1}), however, than the tuning range of the FWM vuv radiation.

We observe in addition that not only the Stokes lines but also the vuv *B-X* lines are tunable over a range of ~ 10 cm^{-1} with irradiation of the ir laser. The effect may be due to stimulated two-photon emission (TPE) [16] [Fig. 1(e)] as we will discuss below.

The rest of the paper is organized as follows. In Sec. II the phase mismatch Δk, the vuv absorption cross section σ_{vuv}, the nonlinear susceptibility $\chi^{(3)}_{FWM}$ responsible for the four-wave mixing process, the Raman gain factor g_r, and the small-signal gain factor g_{TPE} for stimulated TPE will be calculated. The small-signal gain coefficient for PFWM in case of phase matching as well as the intensity of the vuv wave in case of FWM as a function of the irradiated ir laser frequency will be calculated using these quantities. In Sec. III the experimental setup is described. The experiments and the results are outlined in Sec. IV, and a comparison is made with the theoretical results obtained in Sec. II. This section is subdivided into part A, where experiments are described with irradiation of the vuv laser solely, and section B, with additional irradiation of ir laser radiation. In Sec. V, special aspects of the experimental results are discussed and an outlook to possible future experiments is given. Section VI gives a brief summary of the results.

II. THEORY

Several nonlinear processes are connected with two-photon excitation of H_2 (FWM, PFWM, SRRS, SEHRS, and possibly TPE). Theoretical aspects of these processes have been extensively discussed in the literature and can be found in standard textbooks [17–19], so that we can restrict ourselves to the calculation of the linear and nonlinear quantities involved. In contrast to the majority of the references, we will use SI units throughout. We start with a calculation of quantities related to parametric four-wave mixing and four-wave mixing.

In the case of FWM ω_{uv} and ω_{ir} are irradiated and ω_{vuv} is generated (Fig. 1). With the assumption of negligible attenuation of the irradiated waves, one obtains in the approximation of plane waves for the intensity of the vuv radiation the following expression [17]:

$$I_{\mathrm{vuv}}=\frac{\omega_{\mathrm{vuv}}^2 N^2 l^2 I_{\mathrm{uv}}^2 I_{\mathrm{ir}}}{(2c)^4 n_{\mathrm{vuv}} n_{\mathrm{uv}}^2 n_{\mathrm{ir}}}|\chi_{\mathrm{FWM}}^{(3)}/\epsilon_0^2|^2 F(\Delta kl,\alpha l) \times\exp(-\sigma_{\mathrm{vuv}}NL) , \quad (1)$$

with

$$F(\Delta kl,\alpha l)=\frac{\sinh^2(\alpha l/2)+\sin^2(\Delta kl/2)}{(\alpha l/2)^2+(\Delta kl/2)^2}\exp(-\alpha l) ,$$

and $2\alpha=\sigma_{\mathrm{vuv}}N$.

Here, ω_{vuv} is the frequency of the vuv wave; $\chi_{\mathrm{FWM}}^{(3)}$ is the nonlinear susceptibility per molecule for difference frequency mixing convolved with the Doppler profile of the gas and the autocorrelation function of the spectral profile of the irradiated uv wave; σ_{vuv} is the absorption cross section for the vuv wave; N is the particle density; l is the interaction length; L is the path length through the absorbing medium between the interaction zone and detector, and $\Delta k=2k_{\mathrm{uv}}-k_{\mathrm{ir}}-k_{\mathrm{vuv}}$ is the phase mismatch. It is assumed that the interaction takes place over a short range of length l localized at the focus of the irradiated waves, whereas the vuv wave has to travel a considerably larger distance L through the medium to the detector. For $l\ll L$ or $\alpha\ll 1$, F can be approximated by $F\simeq\mathrm{sinc}^2(\Delta kl/2)$.

In the case of parametric four-wave mixing, the ir and vuv waves build up from quantum noise. The generation of both waves is immediately coupled. The situation is analogous to the well-known effect of optical parametric fluorescence in solids. The results for the OPF process can be directly invoked (in the case of negligible absorption of the uv pump wave) by replacing $\chi^{(2)}$ with the corresponding quantity $\chi_{\mathrm{FWM}}^{(3)}$ multiplied by the amplitude of the irradiated uv wave. The resulting equations are identical to the results for PFWM calculations [20]. For the small-signal gain coefficients of the coupled ir and vuv waves one finds

$$g_{\mathrm{PFWM}}^2=g_0^2-\Delta k^2 , \quad (2)$$

with

$$g_0=\frac{\sqrt{\omega_{\mathrm{vuv}}\omega_{\mathrm{ir}}}}{2c^2}N|\chi_{\mathrm{FWM}}^{(3)}/\epsilon_0^2|I_{\mathrm{uv}} . \quad (3)$$

Equation (2) shows that efficient amplification through parametric four-wave mixing is only possible for frequencies with $\Delta k\simeq 0$. Also, in the case of four-wave mixing, efficient vuv generation will not be possible—due to the $\mathrm{sinc}^2(\Delta kl/2)$ dependence—unless Δk is small. For the calculation of Δk the refractive indices $n(\omega)$ at the various frequencies are required since we have $k(\omega)=\omega n(\omega)/c$. Whereas for uv and ir frequencies data for the refractive index (which is only weakly frequency dependent) are available [21], the strongly frequency-dependent refractive index in the vuv has to be calculated.

The vuv frequencies involved are close to X-B absorption resonances, and one can expect a strong depletion of the generated vuv wave. Therefore the absorption cross section has to be calculated in addition.

The refractive index n and the absorption cross section σ_{vuv} are connected with the real and the imaginary part, respectively, of the first-order susceptibility $\chi^{(1)}=\chi'^{(1)}+i\chi''^{(1)}$:

$$\chi^{(1)}=\sum_i \rho_i \sum_k \frac{|\langle i|er|f\rangle|^2}{\hbar(\omega_{if}-\omega-i\gamma_{if}/2)} , \quad (4)$$

and

$$n^2=1+N\chi'^{(1)}/\epsilon_0 ,$$

$$\sigma_{\mathrm{vuv}}=\frac{\omega_{\mathrm{vuv}}}{cn_{\mathrm{vuv}}}\chi''^{(1)}/\epsilon_0 .$$

In these expressions, ρ_i is the relative population of the rotational ground states j_i, ω_{ik} is the single-photon resonance frequency for the transition $i\rightarrow f$, and γ_{if} is the homogeneous linewidth—full width at half maximum (FWHM)—of this transition. This linewidth has a substantial influence on the value of σ_{vuv}. Various broadening mechanisms may be effective (e.g., collisions of neutral H_2 molecules, Stark broadening by photoelectrons). A value of $\gamma_{ik}=\gamma=3\times10^9$ s^{-1}—this is nearly twice the natural linewidth—was chosen from comparison with the experimental results. The transition matrix elements can be derived from the absorption oscillator strengths f_{if} of the vibrational transitions between two electronic levels [22]:

$$|\langle i|er|f\rangle|^2=f_{if}\frac{e^2\hbar}{2\omega_{if}m_e} . \quad (5)$$

In order to take account of the rotational structure, these values have to be weighted with the Hönl-London factors for absorption. In Eq. (4) the sum has to be extended over all rovibronic transitions. Measured oscillator strengths have been communicated in Refs. [23–25]. Unfortunately, these data are not complete so that theoretical oscillator strengths and FCC have to be used in the calculation [26–29]. The FCC are proportional to the oscillator strengths. The proportionality factor was found by comparing the calculated FCC with the measured oscillator strengths.

The following hydrogenic states were included: the B state (including the rotational structure) up to $v=17$, the C, B', and D states with vibrational levels up to $v=13$, and the B'' and D' states through an effective level located at 15 eV. In view of the lack of more detailed data, the effective level at 15 eV is assigned an oscillator strength of $f=0.139$ on the basis of the Thomas-Reiche-Kuhn sum rule [22]. The population in the various rotational levels was taken into account up to $j=4$ at a temperature of 300 K. The resonance frequencies were taken from Refs. [30 and 46]. The values calculated according to Eq. (4) were convolved with a normalized Doppler profile for 300 K.

Figure 2 shows the normalized phase mismatch per particle as a function of the vuv frequency and the ir frequency for resonant $Q(1)$ two-photon excitation from $X(0)$ to $EF(6)$ (103 487.08 cm^{-1}) in the vuv frequency range between 91 200 and 91 850 cm^{-1}. [For simplicity we will use the notation $X(0)$ instead of $X(v=0)$ throughout in this paper.] Table I gives a list of the zeros of Δk. Six

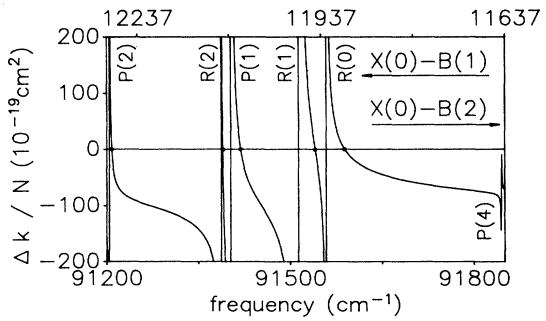

FIG. 2. Calculated Δk distribution, normalized per particle. The zeros of the vertical lines correspond to single-photon resonances; the adjacent zeros located at slightly higher vuv frequencies lead to phase matching. These frequencies are indicated by points on the abscissa. The scale on top of the figure indicates the corresponding ir frequency for FWM or PFWM with resonant $Q(1)$ excitation to $EF(6)$.

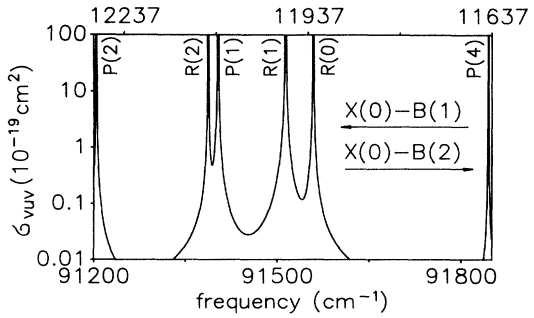

FIG. 3. Calculated absorption cross section as a function of frequency. The frequency scales are the same as in Fig. 2.

$X(0)$-$B(1)$ resonances are within the spectral range shown in Fig. 2: $R(0)$, $R(1)$, $P(1)$, $R(2)$, and $P(2)$. The $P(4)$ resonance of the $X(0)$-$B(2)$ transition is rather weak.

The result of the calculation of the absorption cross section is represented in Fig. 3 for the same frequency interval. The resonances mentioned are obvious. We note that the absorption coefficient at the zero of Δk at 91 540.5 cm^{-1} (or at 11 946.6 cm^{-1} in the IR) amounts to $\sigma_{vuv}=0.117\times10^{-19}$ cm^2. For the situation of our experiment (namely, a pressure of 300 mbar and an optical path length $L=190$ cm), a transmission of 1.7×10^{-8} results. Nevertheless, absorption is negligible at this frequency over the interaction length of approximately 1 cm. We can therefore expect this vuv radiation to be detectable only at pressures below several 10 mbar, although this wave can propagate over the interaction range practically unabsorbed even far beyond this pressure.

TABLE I. Comparison of calculated and measured phase-matching frequencies. The calculated frequencies are independent of the specific two-photon excitation. For the measured frequencies the superscript a indicates the observation of the PFWM line in the ir and b the observation of SRRS lines in the vuv in connection with FWM.

Resonance transition	$\tilde{\nu}_{vuv}$ (cm^{-1}) Calculated	Measured after $Q(j)$ excitation $Q(0)$	$Q(1)$	$Q(2)$	$Q(3)$
$X(0)$-$B(0)$			from $X(0)$ to $EF(6)$		
$F(0)$	90 249.8	90 247.8[a,b]	90 248.8[b]		
$F(1)$	90 215.7	90 209.8[b]	90 213.4[a,b]		
$P(1)$	90 093.5		90 092.5[b]		
$R(2)$	90 081.3		90 081.4[b]	90 081.2[a,b]	
$P(2)$	89 890.1				
$R(3)$	89 882.4				
$P(3)$	89 615.8				
$X(0)$-$B(1)$			from $X(0)$ to $EF(6)$		
$R(0)$	91 588.8	91 588.4[a,b]	91 589.3[b]		
$R(1)$	91 540.5	91 541.0[a,b]	91 540.1[a,b]	91 539.7[b]	
$P(1)$	91 419.0	91 421.0[b]	91 418.3[b]	91 419.3[b]	
$R(2)$	91 389.6		91 389.9[b]	91 389.4[a,b]	
$P(2)$	91 208.5				
$R(3)$	91 148.1				91 183.6[a]
$P(3)$	90 930.3				
$X(0)$-$B(2)$			from $X(0)$ to $EF(7)$		
$R(0)$	92 919.7				
$R(1)$	92 824.4				
$P(1)$	92 706.7				
$R(2)$	92 662.8			92 662.5[a]	
$P(2)$	92 490.7				
$R(3)$	92 451.9				92 451.4[a]
$P(3)$	92 209.5				

For the calculation of $\chi^{(3)}_{\rm FWM}$, the two-photon resonance X-EF and a series of X-B resonances have to be taken into account. We expect these resonances to dominate and consider therefore only the resonant part of $\chi^{(3)}_{\rm FWM}$. Following Ref. [17] we obtain for the present case of two-photon resonance the following expression for $\chi^{(3)}_{\rm FWM}(\omega_{\rm vuv}=2\omega_{\rm uv}-\omega_{\rm ir})$:

$$\chi^{(3)}_{ijkl}=\frac{\rho_g}{2j_g+1}\sum_m \frac{(M^a_{\rm hg})^*_{ij}(M^s_{\rm hg})_{kl}}{\hbar(\Omega_{\rm hg}-2\omega_{\rm uv}-i\Gamma_{\rm hg}/2)}\ , \tag{6}$$

and

$$(M^a_{\rm hg})_{ij}=\sum_n \frac{\langle h|er_{\rm ir}|n\rangle\langle n|er_{\rm vuv}|g\rangle}{\hbar(\omega_{\rm vuv}-\omega_{ng})} \tag{7}$$

and

$$(M^s_{\rm hg})_{kl}=\sum_n \frac{\langle h|er_{\rm uv}|n\rangle\langle n|er_{\rm uv}|g\rangle}{\hbar(\omega_{\rm uv}-\omega_{ng})}\ . \tag{8}$$

In these equations, ρ_g describes the relative thermal population of the ground-state rotational level j_g from which the two-photon excitation starts; $\sum_m$ refers to the summation over all $2j_g+1$ degenerate states of this rotational level; $\sum_n$ indicates summation over all rotational-vibrational levels of all electronic molecular states; $\Omega_{\rm hg}$ is the resonance frequency for two-photon excitation into the rotational vibrational level h of the electronic EF state; and $\Gamma_{\rm hg}$ is the homogeneous linewidth of this transition. ω_{ng} refers to the corresponding single-photon resonances. $(M^s_{\rm hg})_{kl}$ describes the "two-photon absorption" and $(M^a_{\rm hg})_{ij}$ the corresponding "emission." The equation for $(M^s_{\rm hg})_{kl}$ takes into account that both uv waves are supplied by one single pump source. The subscripts $ijkl$ designate the various directions of polarizations of the four waves. We will consider only the cases $zzzz$ and $zzxx$, since in the present case both the uv and ir radiation are linearly polarized. Furthermore, we will consider only Q transitions between states $X(0)$ and $EF(v)$. In the general case one would have to sum up the various contributions of the two-photon transitions. In case of resonant or quasiresonant pumping of a two-photon transition, however, the contributions of the nonresonant $\chi^{(3)}_{\rm FWM}$ components lead to a substantial value only if there is a single-photon resonance in the vuv that can compensate for the lack of the two-photon resonance. The absorption connected with single-photon resonances would prohibit the propagation of the vuv wave, however, so that we will not include those contributions in the calculation of the vuv intensity.

Since the uv wavelength at 193 nm is far below any single-photon resonance, the frequency denominators for the various rotational branches within a single electronic vibrational transition in $(M^s_{\rm hg})_{kl}$ are approximately equal. In this case the rotational transition moments can be separated from electronic vibrational moments:

$$(M^s_{\rm hg})_{zz}=\sum_\Lambda \sum_{(j,m)_n} \langle(\Lambda jm)_h|e_z|(\Lambda jm)_n\rangle \times\langle(\Lambda jm)_n|e_z|(\Lambda jm)_g\rangle M^\Lambda_{\rm hg}\ . \tag{9}$$

Λ stands for the quantum number describing the projection of the electronic angular momentum onto the molecular axis, $M^\Lambda_{\rm hg}$ is the sum over all vibrational states of all electronic states of the same quantum number Λ, and e_z is the z component of the unit vector. The representation of the rotational matrix elements leads, in general, to a complicated expression depending on Λ, j, and m. In case of the H_2 molecule, one has to include only Σ and Π states. The matrix elements M^Σ_{EFX} and M^Π_{EFX} have been calculated in Ref. [31] for the transition $X(0)$-$EF(6)$. We note that the values given in Table 2 of Ref. [31] contain a degeneracy factor of 2 that does not apply here. Furthermore, all matrix elements in Ref. [31] are too large by a factor of 2—as was already pointed out in Ref. [32]. Thus we obtain $M^\Sigma_{ERX}/\epsilon_0=-2.02\times10^{-24}$ cm^{-3} and $M^\Pi_{EFX}/\epsilon_0=-2.095\times10^{-24}$ cm^3, respectively. These two matrix elements are almost equal, and we approximate them by $M^\Sigma_{EFX}=M^\Pi_{EFX}=M_{EFX}=-2.06\times10^{-24}$ cm$^3\epsilon_0$. In this case the summation over the rotational matrix elements for Σ and Π transitions yields the value 1, and therefore no j or m dependence remains. The two-photon transition matrix elements have been calculated in Ref. [31] for various values of j, and the same result is obtained throughout. Our values calculated with the approximation mentioned differ from these results by less than 1%.

In view of the lack of an m dependence, all $(2j+1)$ degenerate sublevels are equally populated and we have an isotropic situation with $\chi^{(3)}_{\rm FWM}$ independent of the direction of polarization of the ir laser. It is therefore sufficient to calculate $(M^a_{\rm hg})$ for an arbitrary direction (e.g., zz). One obtains

$$\sum_m (M^a_{\rm hg})=\tfrac{1}{3}\sum_v \left[\frac{j}{\hbar(\omega-\omega_v^-)}+\frac{j+1}{\hbar(\omega-\omega_v^+)}\right]\tilde{M}_v\ . \tag{10}$$

Only the lower rovibrational states of the electronic B state have to be taken into account as intermediate levels for the calculation of $(M^a_{\rm hg})$, since only these yield a resonant contribution. The vibrational transition moments M_v cannot be taken as given in Ref. [31], however, since they were calculated for the uv frequency of the pump laser and not for the vuv frequencies. We therefore have to single out the frequency denominator: $\tilde{M}_v=M_v\hbar(\tilde{\omega}-\omega_v)$ with $\tilde{\omega}$ being the uv frequency of the

TABLE II. Transition moments $\tilde{M}_v$ calculated after Ref. [31] and corresponding ir and vuv frequencies [$EF(6)$-$B(v)$ and $B(v)$-$X(0)$, respectively].

v_B	$\tilde{M}v/\epsilon_0$ (10^{-43} cm^3 J)	$\tilde{\nu}_{\rm ir}$ (10^3 cm^{-1})	$\tilde{\nu}_{\rm vuv}$ (10^3 cm^{-1})
0	2.83	13.3	90.2
1	−7.45	12.0	91.5
2	−1.97	10.7	92.8
3	1.73	9.5	94.0
4	2.45	8.3	95.2
5	9.45	7.1	96.4
6	11.55	6.0	97.6
7	4.54	4.9	98.7
8	2.10	3.8	99.8

two-photon excitation and ω_v the resonance frequency for the transition $X(0)$-$B(v)$. The values calculated in this manner are given in Table II together with the corresponding ir and vuv frequencies of EF-B and B-X transitions. The frequencies ω_v^+ and ω_v^- designate the resonance frequencies $X(0,j)$-$B(v,j\pm1)$.

In order to calculate the absolute intensity, it is necessary to convolve the expression for $\chi^{(3)}_{\rm FWM}$ with the Doppler profile and the autocorrelation function of the uv laser. This leads to an expression which, in general, cannot be treated analytically. In Ref. [33], however, an approximation is given that is valid for the case of a Gaussian spectral profile of the uv laser and the Doppler width exceeding by far the homogeneous linewidth. The convolution involves only the frequency denominator of Eq. (6). Therefore, for exact two-photon resonance and the condition mentioned above, the following substitution applies in the expression for $|\chi^{(3)}_{\rm FWM}|^2$ [Eq. (6)]:

$$|1/(\Omega_{\rm hg}-2\omega-i\Gamma_{\rm hg}/2)|^2 \rightarrow G/\Delta\omega_d^2 , \tag{11}$$

with

$$G=32\ln(2)\{(2/r)\tan^{-1}(r)(1+v^2/4) + (v^2/2)/(1+r^2)-v[\pi/(1+r^2)]^{1/2}\}$$

and

$$v=\sqrt{8\ln(2)}\Gamma_{\rm hg}/\Delta\omega_d,\quad r=[1+(2\Delta\omega_{\rm uv}/\Delta\omega_d)^2]^{1/2} .$$

$\Delta\omega_d=1.7\times10^{11}$ s^{-1} is the Doppler linewidth and $\Delta\omega_{\rm uv}=5.6\times10^{10}$ s^{-1} the uv laser linewidth (FWHM). We choose $\Gamma_{\rm hg}=2\times10^{10}$ s^{-1} in accordance with Ref. [31] and obtain $G=26.4$. The resulting dependence of $\chi^{(3)}_{\rm FWM}$ is represented in Fig. 4 for the case of resonant $Q(1)$ excitation to $EF(6)$ ($\Omega_{\rm hg}=103\,487.08$ cm^{-1}) and transitions involving $B(1)$.

With these parameters the vuv intensity can be calculated as a function of the ir laser frequency. The result is shown in Fig. 5 for $I_{\rm uv}=1\times10^{11}$ W cm^{-2} and $I_{\rm ir}=1\times10^{9}$ W cm^{-2}. The resulting vuv intensity of the order of $\sim10^{11}$ W cm^{-2} exceeds by far the meaningful range since for these intensities more vuv photons would

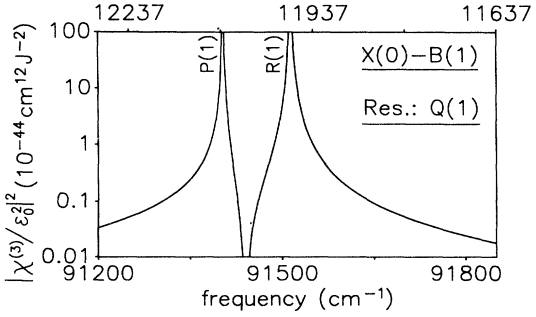

FIG. 4. Calculation of the nonlinear molecular susceptibility for difference frequency mixing with resonance $Q(1)$ two-photon excitation to $EF(6)$ in the frequency range of the $X(0)$-$B(1)$ resonances. Doppler broadening and finite laser linewidth are taken into account. For the frequency scale see Fig. 2.

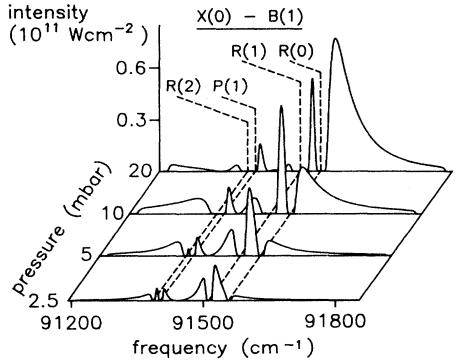

FIG. 5. Calculated vuv intensity in the case of FWM as a function of the vuv frequency for various pressures. The calculation applies to resonant $Q(1)$ excitation to $EF(6)$. The spectral position of the X-B single-photon absorptions are indicated. For details see text.

be emitted than ir photons are irradiated. This contradiction is a consequence of the neglect of saturation effects (e.g., two-photon cancellation [20], self-defocusing, and pump depletion [34]) and of various efficient loss mechanisms (e.g., losses by emission processes like ASE and SEHRS, losses by SRRS, photoionization and dissociation, and depletion of the ground-state population). These limiting processes will be discussed together with the experimental results in Sec. V.

In Eq. (3), g_0 gives the small-signal gain for parametric four-wave mixing for the case of exact phase matching, neglecting absorption, and the limiting effects mentioned. Note that g_0 depends only linearly on N and $|\chi^{(3)}|$. In Table III small-signal gain coefficients g_0 are given for the case of resonant $Q(1)$ excitation. It is therefore reasonable to expect gain values in excess of e^{30} at pressures above 100 mbar, where the factor of 30 is an order of magnitude argument for the detection of a signal to build up from noise [18].

Next, we want to study the effect of stimulated resonant Raman scattering. We have shown that the vuv radiation generated by PFWM is slightly above X-B resonance transitions. This leads to both a strong increase of the Raman-scattering cross section and a change of the usual Raman selection rules. In the usual case of SRS, i.e., far away from resonances, we have $\Delta v=\pm1$. In the resonant case, however, the FCC of the resonant inter-

TABLE III. Selected small-signal gain factors (in cm^{-1}) for PFWM for the case of exact phase matching and resonant $Q(1)$ excitation $X(0)$ to $EF(6)$. The corresponding ir and vuv frequencies are indicated. (100 mbar H_2, $I_{\rm uv}=1.0\times10^{11}$ W cm^{-2}.)

$\tilde{\nu}_{\rm ir}$	$\tilde{\nu}_{\rm vuv}$	g_0
11 898.3	91 588.8	43.1
11 946.6	91 540.5	110.2
12 068.1	91 419.0	57.5
12 097.5	91 389.6	119.7

mediate level determine the vibrational ground levels where the scattering processes terminate. We will therefore observe stokes lines to several vibrational ground-state levels ($v=5-8$). Another difference with respect to SRS is the fact that, due to the large value of the scattering cross section, various vibrational as well as rotational transitions will be observed in general (e.g., Q and S transitions). Due to the distant resonances the SRS cross section is largely wavelength independent, whereas in the case of SRRS strong variations with the various rovibronic resonances occur. The Raman gain coefficient is calculated according to [17]

$$g_r=\frac{I_p N\omega_s}{2c^2}\mathrm{Im}(\chi^{(3)}_{\mathrm{SRRS}}/\epsilon_0^2)\ , \tag{12}$$

with

$$\mathrm{Im}(\chi^{(3)}_{\mathrm{SRRS}})=\frac{\pi\rho_g}{\hbar\Delta\omega_r}\left|\sum_n \frac{\langle f|er_s|n\rangle\langle n|er_p|g\rangle}{\hbar(\omega_{ng}-\omega)}\right|^2 .$$

Here, I_p and ω_p stand for the intensity and the frequency of the pump wave; ω_s is the frequency of the Stokes wave, and $\Delta\omega_r$ is the linewidth of the Raman transition. As a consequence of the resonant situation only the two dipole-allowed rotational states of a given vibrational level in the electronic B state have to be summed up. The expression has to be calculated separately for O, Q, and S transitions and for a special combination of initial and final states. The polarization of the waves considered is also of importance. We find

$$\mathrm{Im}(\chi^{(3)}_{\mathrm{SRRS}})=\frac{\pi\rho_j}{\hbar\Delta\omega_r}|\mu(R)_{BX}|^4 q_{0w}q_{vw}\frac{1}{2j+1}\times\sum_m\left|\sum_i\frac{S_{jik}}{\hbar(\omega_{ij}-\omega_p)}\right|^2 , \tag{13}$$

with

$$S_{jik}=\langle k|e_s|i\rangle\langle i|e_p|j\rangle\ .$$

In these expressions, $\mu(R)_{BX}$ is the electronic transition moment, q_{0w} and q_{vw} are the FCC for the transitions $X(0)$-$B(w)$ and $B(w)$-$X(v)$ as given in Ref. [26]; j is the rotational initial state and k the final state with $k=j\pm2$ or 0; S_{jik} is the rotational transition moment containing the polarization directions e_p and e_s of the pump and Stokes waves, respectively. The electronic transition moment shows a weak linear dependence on the internuclear distance R. Since in our consideration $X(0)$ and $B(0$ and 1) are possible initial and intermediate states, a value of $|\mu(R)_{BX}|^2/\epsilon_0=1.37\times10^{-41}$ cm^3 J (applying for a mean internuclear distance of $R=0.1$ nm) has been chosen according to Ref. [23]. For the Raman linewidth we chose $\Delta\omega_r=4.6\times10^{10}$ s^{-1}, according to the Doppler width of the Raman transition. In view of the very large Raman shift of $\sim$25.000 cm^{-1} it seems reasonable to assume that the Doppler width is dominant in this case. Figure 6 shows the results for the transitions $Q(0)$, $Q(1)$, $S(0)$, and $S(1)$ starting at $X(0)$ via $B(1)$ to $X(7)$ for the spectral interval indicated above and for the situation of linear and parallel polarization of the pump and Stokes waves. We

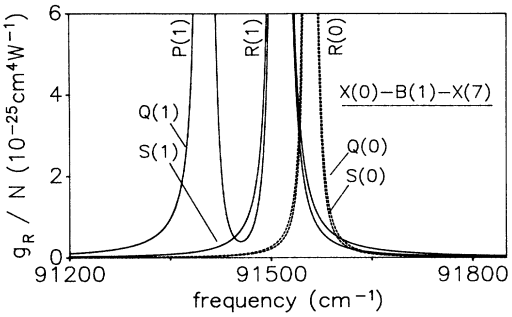

FIG. 6. Calculated small-signal gain coefficient of Q and S transitions for SRRS in the $X(0)$-$B(1)$-$X(7)$ transition path and linearly polarized light. The corresponding R- and P-absorption resonances are indicated. The solid curves refer to scattering at the $j=1$ state and the dashed lines to scattering at molecules in the $j=0$ state.

deduce from this figure that at a pressure of 300 mbar and an interaction length of 1 cm an intensity of the vuv wave at 91 540.5 cm^{-1}, generated by PFWM, of $\sim1\times10^7$ W cm^{-2} is necessary to yield a small-signal gain of e^{30}. In our experimental situation, where the beam cross section in the focal range is $\sim10^{-4}$ cm^2, this leads to a vuv power of $\sim$1 kW. We will show in Sec. IV that this value is reasonable for the PFWM vuv wave.

If the vuv frequency is tuned, generation of a Stokes wave tunable over a certain spectral interval results. As can be seen from Fig. 6, a change in the scattering resonance can occur. In the example given, the Raman cross section decreases rapidly for the $Q(1)$ and $S(1)$ transitions with increasing frequency, whereas an increase for the $Q(0)$ and $S(0)$ transitions is observed. As a consequence, Stokes lines are generated that terminate on o-H_2 levels. These disappear with increasing frequency and lines are generated that terminate on p-H_2 levels. With the frequency increasing further—beyond the $Q(0)$ and $S(0)$ resonance—the process is again reversed since, according to Fig. 6, the $Q(1)$ and $S(1)$ gain coefficients become dominant again.

We learn, in addition, from Fig. 6 that in the case of scattering from the $j=0$ level the Q transition dominates slightly over the S transition. In the case of scattering from the $j=1$ state and frequencies in excess of 91 450 cm^{-1} the situation is reversed. If we have circular polarization there is only a small change for $j=1$ scattering, whereas the intensity situation is reversed for $j=0$ scattering.

The Stokes lines under discussion are clearly different in frequency from the resonance transitions B-X, the so-called Lyman lines. As will be shown in Sec. IV, these Lyman transitions also show tunability over a certain frequency range. On resonance no four-wave mixing is expected due to rapidly rising absorption and large phase mismatch. The tunability of these lines can therefore not be explained by the SRRS process. Stimulated two-photon emission [16] is a possible explanation. The small-signal gain coefficient for this process is calculated in analogy to g_r as

$$g_{\mathrm{TPE}}=\frac{I_{\mathrm{ir}}N^*\omega_{\mathrm{vuv}}}{2c^2}\mathrm{Im}(\chi^{(3)}_{\mathrm{TPE}}/\epsilon_0^2)\ , \tag{14}$$

with

$$\mathrm{Im}(\chi^{(3)}_{\mathrm{TPE}})=\frac{\pi}{\hbar\Delta\omega_{\mathrm{TPE}}}|\mu(R)_{EFB}|^2q_{\mathrm{uw}}|\mu(R)_{BX}|^2q_{wv}\frac{1}{2j+1}\times\sum_m\left|\sum_i\frac{S_{jik}}{\hbar(\omega_{ij}-\omega_{\mathrm{vuv}})}\right|^2 .$$

ω_{vuv} stands for the vuv wave generated in the TPE process, and S_{jik} is again the corresponding rotational transition moment. The summation over various rotational levels can be omitted in this case, since only frequencies in close vicinity of the resonance ω_{ij} are of interest. The quantity $|\mu(R)_{EFB}|^2q_{61}/\epsilon_0=1.18\times10^{-41}$ cm^3 J was determined on the basis of transition probabilities given in Ref. [35]. The Doppler width yields a linewidth of the transition of $\Delta\omega_{\mathrm{TPE}}=1.3\times10^{11}$ s^{-1}; N^* designates the population of the EF state. For the $Q(1)$ transition from $EF(6)$ to $X(7)$ via $B(1,2)$, we obtain $g_{\mathrm{TPE}}/N^*=1.1\times10^{-12}$ cm^2 for a detuning from the B-X resonance of $|\omega_{ij}-\omega_{\mathrm{vuv}}|=5.0\times10^{11}$ s^{-1} (corresponding to 2.7 cm^{-1}) and an irradiated infrared intensity of $I_{\mathrm{ir}}=1.0\times10^9$ W cm^{-2}. A small-signal gain of e^{30} is therefore obtained with an interaction length of 1 cm at a density in the excited state of 3×10^{13} cm^{-3}. In view of the large value of the two-photon absorption coefficient and particle densities of several 10^{18} cm^{-3} in the ground state, this value sounds realistic. If we compare this value with the coefficient for the small-signal gain of ASE radiation in the EF-B transition, we obtain

$$g_{\mathrm{ASE}}=\frac{N^*\pi\omega_{\mathrm{ASE}}}{c\hbar\Delta\omega_{\mathrm{ASE}}}(|\mu(R)_{EFB}|^2/\epsilon_0)q_{uw}\sum_m\frac{|S_{ji}|^2}{2j+1}\ . \tag{15}$$

The same small-signal gain of e^{30} is obtained for the $P(2)$ transition $EF(6)$-$B(1)$ ($\sum_m|S_{ji}|^2=\frac{2}{3}$) with a linewidth of the ASE radiation of $\Delta\omega_{\mathrm{ASE}}=1.9\times10^{10}$ s^{-1} (Doppler width) at a density $N^*=9\times10^{13}$ cm^{-3}, i.e., a similar density in the excited state. With irradiation of infrared radiation several wave numbers off resonance, stimulated two-photon emission and amplified spontaneous emission are processes of comparable efficiency and should therefore both be observable.

III. EXPERIMENT

The experimental setup comprises two laser systems to supply the uv and ir radiation fields, a hydrogen cell, and a spectrograph followed by the detection system (Fig. 7). The first laser system generates uv radiation around $\lambda\sim193$ nm necessary for the two-photon excitation. It consists of a XeCl excimer laser (Lambda Physik, EMG 200 MSC), a three-stage dye laser (Lambda Physik, FL 3002 with dye QUI), which yields pulses of approximately 15-ns duration containing ~35 mJ at $\lambda\sim370$ nm and an ArF amplifier (Lambda Physik, EMG 200 MSC). The dye-laser output beam is expanded 1:2 and is focused into a LN_2-cooled H_2-filled Raman cell ($p=700$ mbar) with a $f=60$-cm lens. The sixth anti-Stokes component at

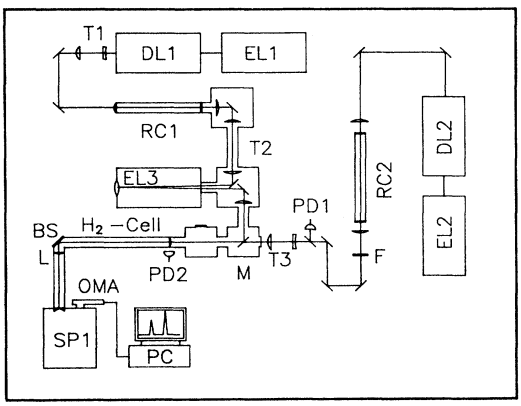

FIG. 7. Scheme of experimental setup. Legend: DL1 and DL2: dye lasers; EL1 and EL2: XeCl excimer lasers; EL3: ArF excimer laser; RC1 and RC2: Raman cells; SP1 Czerny-Turner spectrograph; OMA: optical multichannel analyzer; T1,T2,T3: beam expanders; F: color filter; M: dielectric mirror; BS: beam splitter; L: LiF lens; PD1,PD2: photodiodes.

$\lambda\sim193$ nm ($E\sim20$ μJ) is singled out by dielectric mirrors. The beam diameter is reduced by an inverse telescope by a factor of 2 down to approximately 3 mm. The radiation passes the discharge channel of the ArF amplifier and meets the convex surface of a MgF_2 lens ($r=0.8$ m) acting at the same time as a window of the discharge chamber of the laser. The reflected diverging radiation is amplified in a second pass, and is collimated by a quartz lens after reflexion from a dielectric mirror. After amplification the maximum energy amounts to $E\sim50$ mJ at a spectral width of $\Delta\tilde{\nu}_{\mathrm{uv}}\sim0.3$ cm^{-1}. The radiation is linearly polarized and is tunable over a spectral range of approximately $\Delta\tilde{\nu}\sim450$ cm^{-1}. About 40% of the energy is contained in a short spike of $\Delta\tau\sim1$ ns (FWHM) at the leading edge of the 10-ns pulses. Time-resolved measurements show that all observed nonlinear effects are connected to the radiation contained in this short spike. The beam cross section is 2×1 cm^2, and a beam divergence $D\sim50$ μrad is measured. All optical components are mounted in evacuable chambers connected by tubes in order to avoid absorption in the Schumann-Runge bands of atmospheric O_2.

The second laser system generates ir radiation. It consists of the same type of excimer laser and dye-laser combination as mentioned above and generates radiation at $\lambda\sim560$ nm (fluoresceine 27) or $\lambda\sim620$ nm (sulforhodamine B). This visible radiation is Stokes shifted in a H_2-filled high-pressure Raman cell ($f=80$ cm, 40 bar). The first Stokes component is singled out by a color filter (Schott, RG 645) and dielectric mirrors and is expanded (1:4) to a beam diameter of ~1 cm. At $\lambda\sim750$ and 840 nm, respectively, pulses of duration $\Delta\tau_{\mathrm{ir}}\sim10$ ns with pulse energies of $E\sim5$ mJ, a spectral width of $\Delta\tilde{\nu}_{\mathrm{ir}}\sim0.3$ cm^{-1}, and a beam divergence of $D\sim50$ μrad are obtained. In contrast to direct generation of radiation in the spectral range mentioned with dye lasers [where a broadband background contribution (ASE) is practically

unavoidable] this method has the advantage that, due to the nonlinear step, no background is present. This is important especially for the selective study of processes where excitation takes place in spectrally neighboring intervals, e.g., resonant ASE transitions and four-wave mixing with phase matching only a few wave numbers separated from the resonance. The ir radiation generated is linearly polarized transverse to the direction of polarization of the uv radiation.

Both laser beams—the uv pump beam at $\lambda \sim 193$ nm and the ir radiation—are combined by a dielectric mirror and are focused by a quartz lens ($f = 90$ cm) into the stainless-steel hydrogen cell. The beam expanding telescope of the ir source is used to warrant the spatial overlap of the two laser foci. The beam waist at the focus is $2w_0 \simeq 2fD \simeq 0.01$ cm and an interaction length of $2z_0 \simeq 2Df^2/w_{01} \simeq 1$ cm is estimated. Taking into account reflexion losses at the various optical components, focal intensities (in the center of the tuning curves of the laser output) of $I_{uv} = 1.5 \times 10^{11}$ W cm^{-2} and $I_{ir} = 3.5 \times 10^9$ W cm^{-2} are calculated. Two vacuum photodiodes (Valvo, XA 1003 and UVHC 20) measure the pulse shapes in the ir and uv and are used to monitor the temporal overlap in connection with a 1-GHz oscilloscope (Tektronix 7104).

The radiation leaving the focal range is partially reflected from a glass plate under 45° and is focused by a LiF lens ($R = 10$ cm) onto the entrance slit of a 0.75-m Czerny-Turner vacuum spectrograph (Spex, SP1500, grating 1200 mm^{-1}). The partial reflexion from the glass plate avoids focusing of the full uv power onto the spectrograph slit. A homemade optical multichannel analyzer with a fiber-optical image intensifier follows the exit slit of the spectrograph. A 25-μm plastic scintillator foil (NE 102A) is attached to the fiber-optic entrance plate of the image intensifier so that this detector is sensitive from vuv to near ir wavelengths. For the measurements in the near vuv (130–160 nm) the spectrograph is set to second, third, or fourth order to increase the effective resolution. A different arrangement is used to detect the short-wavelength vuv radiation around 109 nm. This became necessary because the transmission of the LiF optical component is completely insufficient, and, in addition, the Czerny-Turner spectrograph exhibits substantial reflexion losses for wavelengths below 130 nm. In the modified arrangement the vuv radiation generated in the focus is imaged by a concave glass plate ($r = 50$ cm) under 90° onto the entrance slit of a $f = 20$-cm vuv double monochromator (2×Minuteman 302VM, grating 600 mm^{-1}). This method of imaging entails a large astigmatism and leads to a large focal spot at the entrance slit so that only part of the available optical power is detected. A sodium salicylate-coated glass plate follows the exit slit of the monochromator. The fluorescence light generated in the sodium salicylate layer is detected by a photomultiplier (Hamamatsu QB 9634). The entire optical path between the focus in the hydrogen cell to the scintillator is kept in H_2, so that no window is necessary. The optical path from the focus to the scintillator amounts to 190 cm.

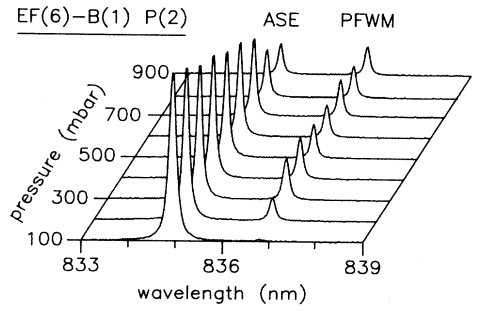

FIG. 8. Section of the ir spectrum for resonant $Q(1)$ excitation to $EF(6)$ as a function of the H_2 pressure (wavelengths in air).

IV. MEASUREMENTS AND RESULTS

A. Self-induced effects

We start with the description of measurements performed without irradiation of additional ir laser radiation. In this case only the PFWM lines (ir) and the Stokes lines generated by SRRS (near vuv) are observed. The detection of the vuv counterpart of the ir PFWM line is not possible since PFWM develops only at pressures in excess of several hundred mbar. In this pressure range (see Sec. II) the H_2 absorption along the optical path to the detector (~ 190 cm) is very effective.

ASE transitions *EF-B* are observed already at H_2 pressures as low as 1 mbar. In parallel to the observation of these ir transitions in the spectral range between 750 and 950 nm, additional redshifted lines are observed at pressures in excess of 100 mbar. The most intense of these additional lines is close to the $EF(6)$-$B(1)P(2)$ transition and exhibits a shift of $\Delta\tilde{\nu} = -26.7$ cm^{-1} (see Fig. 8). In the following we will mainly refer to this line. The intensity in these additional lines stays almost constant with increasing pressure, whereas the intensity of the ASE lines decreases. At high pressures (> 1 bar) the intensity of the additional lines can even exceed that of the regular transitions. We observe such satellites for each regular H_2 line. They are present only in the direction of propagation of the irradiated uv radiation but cannot be observed in backward direction. The regular lines are observed in both directions, with the backward intensity increasing, however, in contrast to the forward intensity with increasing pressure over a large pressure range up to ~ 700 mbar. If the backward intensity is maximum, it exceeds the maximum of the forward intensity by approximately one order of magnitude.

The oberved ir satellite lines and the corresponding vuv waves in the spectral range between 108 and 111 nm are generated by parametric four-wave mixing. The phase-matching frequencies of the vuv lines are several wave numbers higher than the frequencies of the regular *X-B* transitions. The good agreement between the calculated and the measured frequencies is demonstrated in Table I. For the $X(0)$-$B(1)$ and $X(0)$-$B(2)$ transitions the agreement is clearly better than 1 cm^{-1}, but for the $X(0)$-

$B(0)$ resonance the calculated values are slightly too high throughout. In case of the $X(0)$-$B(0)$ transitions the deviations clearly exceed our estimated experimental error ($<\pm 1$ cm^{-1}). Assigning the oscillator strength a numerical value increased by 50% leads to good agreement between calculation and measurement. It seems, however, very unlikely that the oscillator strength is in error by such an amount, because the experimental and theoretical values known from literature [23,28,47] agree all very well.

With tuning of the uv pump laser both the frequencies of the regular and the PFWM lines vary with the factor 2 of the uv frequency change (see Fig. 9). In the first case there is a transition from ASE to SEHRS emission. ASE and SEHRS are generated in parallel within the Doppler width of the two-photon resonance (0.9 cm^{-1}). The spectral separation of both lines is difficult to observe, and a superposition of both contributions is measured close to the resonance. Therefore we find a "saddle" in the vicinity of the resonance insted of the linear dependence expected. Maximum intensity is obtained on resonance of the two-photon transition. In the case of PFWM, the phase-matching condition $\Delta k = 0$ is almost independent of the uv and ir frequencies over the tuning intervals mentioned, but it is extremely sensitive with respect to changes in the vuv frequency. The vuv frequency, therefore, stays almost fixed with a change of the uv frequency so that this leads to a change in the observed ir frequency. The intensity exhibits a clear minimum at the two-photon resonance. Losses by other radiative processes seem to quench the buildup of PFWM.

The energy of the various EF-B vibrational transitions was mesued by a pyroelectric detector (Laser precision RJ7200 and RJP735) following an interference filter. The measurements were performed for the transitions $EF(6)$-$B(1)$ with $Q(1)$ excitation. The detector is located behind the beam splitter at the exit of the hydrogen cell, and ~90% of ir radiation emitted in forward direction is detected. The comparison of the energy measurements with the ir spectra measured simultaneously yields for the PFWM line at 11 946.6 cm^{-1} ($\lambda = 836.830$ nm) a fraction of ~10% of the total ir energy at 200 mbar or approximately 1 μJ. The pulse duration $\Delta\tau$ is found to be ≤ 1 ns so that a radiation power $P_{ir} \geq 1$ kW results. Due to the fact that with the emission of an ir photon by PFWM the emission of a vuv photon is connected, the vuv power can be estimated to be $P_{vuv} \geq 8$ kW. With increasing pressure the total energy decreases, but the energy of the PFWM line rises by an additional factor ~2 to a saturation value (see Fig. 8). We conclude therefore that the maximum power in the PFWM vuv line is $P_{vuv} \geq 16$ kW.

Satellite lines are also detected in connection with the Lyman bands $B(v'=1)-X(v''=7$ and 8) (see Fig. 10). They are found blueshifted by the same amount as known from the ir lines. These vuv lines are Stokes lines generated by SRRS of the vuv radiation generated in the PFWM process. The transitions close to the regular ir lines are Q transitions and the ones close to P lines are S transitions. In the example mentioned above, both PFWM and SRRS take place at o-H_2 in the $X(0,1)$ state. The intensity of the PFWM vuv wave field in the focal range ($A \sim 10^{-4}$ cm^2) is deduced from the above-mentioned energy measurements to be $\sim 1 \times 10^8$ W cm^{-2}. This is approximately an order of magnitude above the calculated threshold intensity for the onset of SRRS. In the case of the frequencies considered in Fig. 10, the gain factor for $j=1$ scattering from o-H_2 is considerably higher than for $j=0$ scattering from p-H_2 (Fig. 6). The Franck-Condon factors are clearly higher for the transitions $B(1)$-$X(7$ and 8) than to the neighboring vibrational levels of the electronic ground state [28]. This explains why these SRRS transitions are generated especially in connection with these levels.

Admixture of other gases (rare gases, N_2 and D_2) allows us to shift the frequencies of the PFWM lines due to changes of the refractive index. The change in freqency depends only on the concentration of the admixed gas in hydrogen and does not depend on the absolute pressure. This is in agreement with the prediction that the PFWM freuqencies are determined by the ratio of refractive-index differences according to

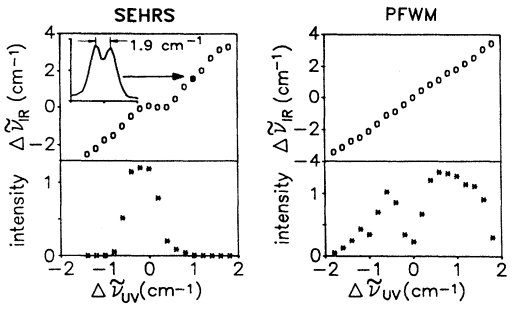

FIG. 9. ir frequency shift $\Delta\tilde{\nu}_{ir}$ of the SEHRS line corresponding to the transition $EF(6)$-$B(1)$ $P(2)$ and of the adjacent PFWM line as a function of the detuning $\Delta\tilde{\nu}_{uv}$ of the pump laser from the $Q(1)$ two-photon resonance to $EF(6)$ at 1000-mbar H_2. In the lower section the corresponding line intensities are displayed. In the case of SEHRS in the vicinity of the resonance ASE and SEHRS are superimposed. An ASE-SEHRS double line, observed at $\Delta\tilde{\nu}_{uv} = 1$ cm^{-1} (the corresponding point in the tuning curve is marked by a dark dot), is shown in the inset. The measured separation of the two lines is 1.9 cm^{-1}.

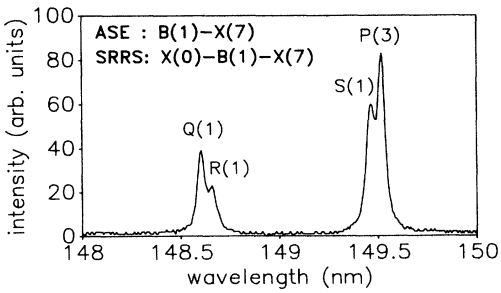

FIG. 10. Section of the vuv spectrum in the case of resonant $Q(1)$ excitation to $EF(6)$ at 400-mbar H_2. The vuv lines shown are generated as a consequence of the ir lines shown in Fig. 8 by ASE starting at $B(1)$ or by SRRS of the PFWM vuv wave.

$$\frac{\omega_{vuv}}{\omega_{ir}} = \frac{n_{uv} - n_{ir}}{n_{vuv} - n_{uv}} \quad . \tag{16}$$

With the exception of He and Kr, all gases investigated (He,Ne,Ar,Kr,Xe,N_2,D_2) lead to a frequency shift towards the neighboring H_2 resonances. In case of He already very small amounts of admixed gas lead to complete quenching of the output. One can speculate on the formation of H_2-He complexes from B-state H_2 molecules [36]. The influence of admixed Kr is to shift the emission frequency away from resonance. Figure 11 shows the spectral shift $\Delta\tilde{\nu}$ of two PFWM transitions—normalized to the situation of pure hydrogen $\Delta\tilde{\nu}_0$—as a function of the ratio of the admixed gas N_X to the total density $(N_X + N_{H_2})$, where X stands for Ar or Kr. The ir lines and the vuv frequencies of the Q and S Stokes lines terminating at $X(7)$ were measured with the spectrograph grating used in first and fourth order, respectively. The Stokes lines reflect indirectly the tuning behavior of the PFWM vuv wave. The solid lines correspond to theory.

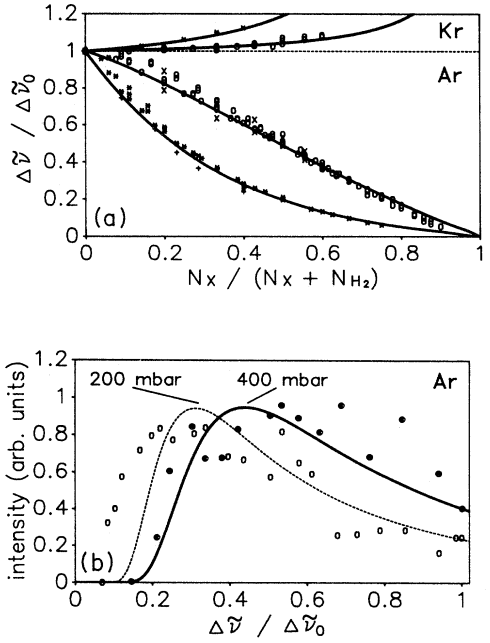

FIG. 11. (a) Tuning behavior of the PFWM lines with admixture of other gases (Kr and Ar) for various H_2 pressures (10–600 mbar). The spectral distance of the lines from the corresponding H_2 resonance is shown, normalized to the case of pure hydrogen, as a function of the fraction of the admixed gas N_x to the total particle density. o: PFWM ir line adjacent to the transition $EF(6)$-$B(1)$ $P(2)$; ×: vuv Stokes lines connected with SRRS $X(1)$-$B(1)$-X(7) of the corresponding PFWM vuv line; *: PFWM ir line adjacent to the $EF(6)$-$B(1)$ $P(1)$ transition; +: vuv Stokes lines connected with SRRS $X(1)$-$B(1)$-$X(7)$ of the corresponding PFWM vuv line. The solid lines represent the calculated dependence. (b) Normalized intensity of the PFWM ir wave adjacent to the $EF(6)$-$B(1)$ $P(2)$ transition as a function of a normalized distance from the resonance in case of tuning by admixture of argon at 200 mbar (○) and 400 mbar (●) of H_2. The dashed (200 mbar) and solid (400 mbar) curves correspond to the dependence described in the text.

The values for the refractive indices of Ar and Xe are taken from Refs. [21,37].

With increasing concentration of admixed gas (with the exception of He and Kr) the intensity of the PFWM line initially increases but goes to zero at still higher concentrations [Fig. 11(b)], whereas the intensity of the regular lines decreases monotonically. The value of $\chi^{(3)}_{FWM}$ increases if the frequency approaches the resonance. This leads to an increased PFWM signal. The absorption cross section, however, is increased too, and therefore beyond a certain frequency a rapid decrease of the signal amplitude results. In the case of optical parametric fluorescence one can show (with some simplifying assumptions) that the intensities of both generated waves are proportional to $|\chi^{(2)}|^2 I_p$ [19]. Applying this result to the PFWM process shows that this expression has to be replaced by $|\chi^{(3)}|^2 I_{uv}^2$. Multiplying by $\exp(-\sigma_{vuv} N l)$ in order to take absorption into account leads to the curves of Fig. 11(b). Except for normalization of intensity, no other fits are used to arrive at these curves.

B. Effects induced by additional ir laser radiation

If the output of the additional ir laser is focused into the H_2 cell, vuv radiation is no longer generated starting from quantum noise, but is stimulated by the laser radiation. The process of four-wave mixing results in a significant increase of the vuv intensity. It is therefore possible to study effects at considerably smaller particle concentrations (typically 10 mbar). This results in advantages with respect to phase mismatch and absorption losses, the latter being reduced by several orders of magnitude (see Sec. II). It is therefore possible to detect vuv radiation in spite of the long path to the detector. In Fig. 12, vuv lines are shown which result in the case of resonant $Q(1)$ excitation to $EF(6)$ at a H_2 pressure of 10 mbar for various ir laser frequencies. Although these lines are separated by ~ 100 cm^{-1}, their wavelength separation is only ~ 0.1 nm. The small dispersion of the short focal-length monochromator (4 nm/mm) complicates a precise wavelength measurement, but the tuning behavior of the vuv frequency with the frequency of the infrared laser is obvious, however.

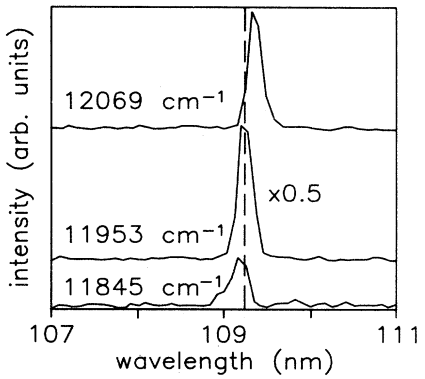

FIG. 12. FWM vuv line for resonant $Q(1)$ excitation to $EF(6)$ for 10-mbar H_2 for various frequencies of the irradiated ir laser. The intensity of the line in the center of the figure has been multiplied by 0.5.

By setting the monochromator slits to a rather wide spacing (0.3 mm), it is possible to record the intensity of the vuv radiation over a substantial spectral interval (1000 cm^{-1}) without readjusting the monochromator setting. The monochromator serves as a narrow-bandwidth spectral filter in this case. The frequency of the vuv radiation is determined from the laser frequencies. In Fig. 13 vuv intensities are shown for various H_2 pressures at resonant $Q(1)$ excitation to $EF(6)$ and the ir laser tuned correspondingly. A comparison of Fig. 13 with the theoretical curves in Fig. 5 shows good agreement, so that the assumptions made in the calculation, e.g., concerning l and σ_{vuv}, seem to be justified. The values for l and σ_{vuv} are very sensitive and can be varied only in an interval of not more than $\pm 10\%$ to yield good agreement with the experiment. Intensity fluctuations in the measured spectra are mainly due to intensity fluctuations of the uv laser. The largest tuning range amounting to approximately 600 cm^{-1} results at a pressure of 10 mbar. FWM is not possible directly on the resonances shown in Fig. 13. Also in the neighborhood of these resonances, even at low pressure, absorption is clearly still effective. Considering, e.g., the two peaks on the left- and right-hand sides of the $R(0)$ resonance (Δk has zeros here, see Fig. 2), one notices that the intensity ratio is inverted when going from 10 to 20 mbar. This is in agreement with the calculations displayed in Fig. 5 and leads to the conclusion that the absorption cross section calculated on the basis of an assumed linewidth of $\gamma = 3 \times 10^9$ s^{-1} is probably quite reasonable.

No attempt was made so far to measure the energy of the FWM vuv wave directly. It is likely, however, that, due to various limiting processes, a value below that calculated in Sec. II does apply. Possible candidates for such processes will be discussed in Sec. V. The energy is expected to be clearly above the value mesured for PFWM, because the intensity of the SRRS lines is considerably increased with irradiation of the ir laser. We therefore expect energies in excess of 10 μJ and power above 10 kW in the vuv for the case of FWM at frequencies where phase matching is effective.

Stimulated resonant Raman scattering, discussed so far

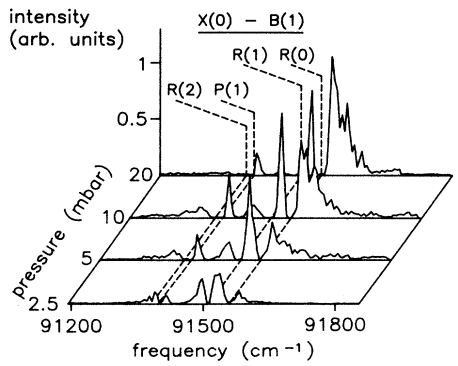

FIG. 13. vuv intensity in the case of four-wave mixing for various pressures as a function of the vuv frequency in the case of resonant $Q(1)$ excitation to $EF(6)$. The vuv frequency is calculated from the frequency of the irradiated waves. The positions of the X-B single-photon absorptions are indicated.

in connection with PFWM, is also present in case of FWM with even higher amplitudes due to the expected higher intensity of the vuv wave. Besides the Stokes transitions already reported in connection with PFWM, several other new lines can be observed in this case. At the appropriate frequency setting of the ir laser it is possible, e.g., to observe four-wave mixing in o-H_2 and subsequent SRRS in p-H_2 (and vice versa). The parallel occurrence of SRRS from various rotational ground levels and scattering of different vuv waves, generated by FWM as well as by PFWM, can lead—together with the ASE lines—to rather complex spectra as can be seen from Fig. 14(a). A vuv wave is generated by FWM in o-H_2 at 91 592.8 cm^{-1} by resonant $Q(1)$ two-photon excitation and ir irradiation at 11 894.3 cm^{-1}. vuv radiation at 91 540.5 cm^{-1} is generated by PFWM. In addition, resonant ASE transitions in the ir and near vuv occur. These lines are indicated by $R(1)$, $P(1)$, and $P(3)$ referring to the transition $B(1)$-$X(7)$ in Fig. 14(a). The FWM- and PFWM-generated vuv waves are responsible for the subsequent generation of SRRS Stokes waves by scattering from H_2 in the ground state $j=0$ (p-H_2) and $j=1$ (o-H_2). The Raman gain factor at the FWM frequency is almost the same for both scattering processes (Fig. 6). Q and S transitions are present in each case so that, in addition to the three regular ASE lines, eight Stokes lines can be observed; not all of them are resolved, however, in Fig. 14(a).

With admixture of D_2, additional phase-matching frequencies for FWM in H_2 result. These frequencies are close to D_2 resonances ($\Delta\tilde{\nu} \sim 2$ cm^{-1}). The vuv waves are preferentially scattered at D_2 resonances and therefore Stokes lines from D_2 are observed subsequent to two-photon excitation of H_2 [Fig. 14(b)]. The observed SRRS processes are connected with D_2 $X(0, j=0, 1,$ and $2)$ ground-state levels. With the ir laser set at different frequencies, besides these D_2 lines also Q and S Stokes lines from HD with scattering at $X(0, j=0$ and $1)$ states are present [see Fig. 14(c)]. The corresponding rotational levels of $B(1)$ act as resonant intermediate levels in case of D_2 as well as for HD. Due to different FCC scattering in D_2 terminates at $X(9$ and $10)$ and at $X(8)$ in case of HD. For HD, the frequencies of the vuv waves generated by FWM (frequencies calculated from the laser frequencies) are very close to the HD resonances (~ 0.1 cm^{-1}) which is below our measuring precision (~ 0.3 cm^{-1}) and within the Doppler width of the X-B transitions. Resonant excitation of HD with subsequent ASE emission is therefore also possible. Because the reaction cross sections for reaction of H_2 with D_2 are negligible at room temperature, HD is generated probably by the following processes [38–41]:

(i) $H^+ + D_2 \rightarrow D^+ + HD$ ($\sim 1 \times 10^{-9}$ $cm^3 s^{-1}$),

(ii) $H_2^+ + D_2 \rightarrow H_2D^+ + H$ ($\sim 2 \times 10^{-9}$ $cm^3 s^{-1}$),

(iii) $H_2^+ + H_2 \rightarrow H_3^+ + H$ ($\sim 2.1 \times 10^{-9}$ $cm^3 s^{-1}$),

$H_3^+ + D_2 \rightarrow H_2D^+ + HD$ ($\sim 2 \times 10^{-10}$ $cm^3 s^{-1}$).

The values in parenthesis correspond to the reaction rates

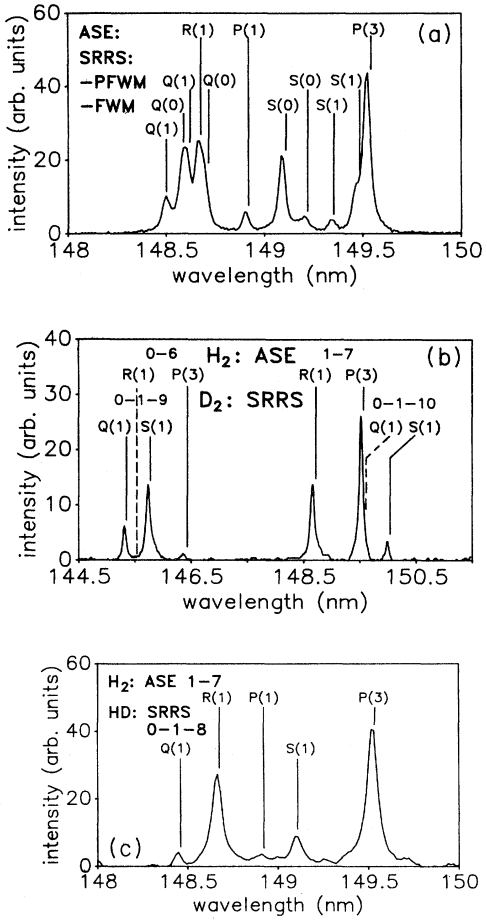

FIG. 14. (a) vuv lines close to the $B(1)$-$X(7)$ transition for resonant $Q(1)$ two-photon excitation to $EF(6)$ and irradiation of an ir wave at 11 894.3 cm^{-1}. The H_2 pressure is 400 mbar (for details see text). (b) vuv lines for the same excitation as in (a), but for a mixture of 160-mbar H_2 and 65-mbar D_2. The ir laser frequency is 11 916.2 cm^{-1}. ASE lines from H_2 and SRRS lines from D_2 are observed. In the case of SRRS the vibrational levels corresponding to the initial, intermediate, and final states are indicated. (c) Same conditions as in (b), but with the irradiated ir frequency at 11 945.3 cm^{-1}. The vuv lines refer to H_2 and HD.

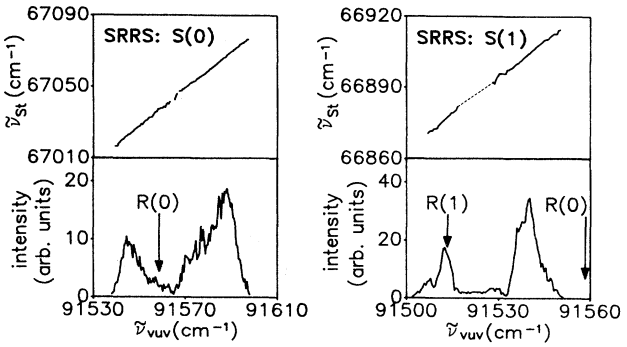

FIG. 15. Tuning behavior of the $S(0)$ and $S(1)$ SRRS Stokes lines $X(0)$-$B(1)$-$X(7)$ in the case of quasiresonant $Q(1)$ two-photon excitation to $EF(6)$ (detuning -1.5 cm^{-1}) as a function of the vuv frequency (calculated from the frequency of the uv laser and the tuned ir laser) at 300 mbar H_2. The ir laser is tuned in 0.5-cm^{-1} steps. The variation of the intensities and positions of the corresponding $X(0)$-$B(1)$ single-photon resonances are displayed in the lower half of the figures. The dashed line in the case of the $S(1)$ tuning curve indicates that in this range no precise wavelength determination was possible because the weak Stokes line connected with FWM and the weak Stokes line connects with PFWM are superimposed.

at room temperature. These rates are large enough to lead to reaction times for the formation of HD from ionic hydrogen of substantially less than 1 ns at neutral particle densities of several 10^{18} cm^{-3}. As shown above, tuning of the ir laser with the frequency of the uv laser fixed leads to tunable vuv radiation by FWM. The corresponding vuv radiation at longer wavelengths generated by SRRS also shows tunability over limited spectral intervals. In Fig. 15 the tuning of the $S(0)$ and $S(1)$ lines belonging to the transition $X(0)$-$B(1)$-$X(7)$ around 149 nm at 200-mbar H_2 is shown as a function of the vuv frequency (calculated from the ir and uv laser frequencies) at quasiresonant (~ 1.5 cm^{-1}) $Q(1)$ two-photon excitation to $EF(6)$. The slight detuning off resonance inhibits the development of strong ASE radiation in the ir and, as a consequence, the efficient population of B-state levels unless the ir laser drives the transition. Therefore, also in the longer wavelength part of the vuv no ASE lines develop.

The Raman cross section for $S(0)$ scattering is maximum at the $R(0)$ resonance and falls off quickly to both sides (Fig. 6). The observation of two maxima is surprising at first, but is explained by the strong absorption of the FWM vuv wave at the $R(0)$ resonance (Fig. 3). Whereas with increasing spectral distance from resonance the cross section decreases, the vuv intensity initially increases (Figs. 5 and 12). The maxima correspond to positions with phase matching (Fig. 2). The intensity at the left maximum is smaller than that of the right since, in addition to the scattering from $j=0$, scattering from $j=1$, which is dominant in this frequency interval, occurs (Fig. 6). The main maximum of the $S(1)$ wave occurs therefore at the same frequency as the left maximum of the $S(0)$ wave and the intensity at this position exceeds that of the $S(0)$ wave. Almost continuous tuning of the $S(0)$ Stokes wave is possible over an interval of 60 cm^{-1}.

The $S(1)$ wave is also tunable over several 10 cm^{-1} and exhibits another maximum at 91 513 cm^{-1}, which is close to the resonance frequency of the transition to $B(1,2)$ (91 514 cm^{-1}). This maximum is surprising since one would rather expect an on-resonance minimum in analogy to the situation with $S(0)$ scattering. We do not expect any FWM due to the large absorption on resonance and therefore there should be no observable Stokes wave. If, in contrast, the maximum were the consequence of resonant population of the $B(1,2)$ state through the ir laser, with subsequent ASE radiation, no tuning of the

corresonding $R(1)$ and $P(3)$ lines would result. This point will be discussed in more detail in the following section.

V. DISCUSSION

A series of PFWM transition with power in the vuv up to 16 kW is observed in the forward direction with respect to the propagation of the uv pump laser light. The intensities of these lines saturate at H_2 pressures in excess of several hundred mbar, whereas the intensities of the regular transitions decrease monotonically in the forward direction and increase initially in the backward direction. In the case of regular transitions with pressures in excess of 100 mbar, a transition from ASE to SEHRS is observed.

The saturation behavior, i.e., the decrease of the intensities in the forward direction and the observed forward/backward asymmetry, is probably due to interference effects in the polarization driving the corresponding processes. Such effects have been investigated both theoretically and experimentally for Na [42,43,20]. The effects discussed for Na are in good agreement with our observations at H_2. The underlying idea assumes that at high intensities the wave fields generated by PFWM may be strong enough to cause excitations of the nonlinear medium and to drive additional strong polarization waves. This leads to interference effects between the polaizations generated by the irradiated and the secondary waves with the consequence that the amplitude of the driving polarizations can be reduced. Both the vuv wave generated by PFWM and the SEHRS and irradiated uv waves lead to excitation of the intermediate B state. Interference of these two processes leads to a reduction of the amplitude of this state in the polarization term. The polarization connected with the SEHRS process is proportional to this amplitude so that in the forward direction SEHRS is suppressed. The polarization propagating in the opposite direction is not affected by these interference effects, so that in this direction SEHRS may develop mainly uninfluenced [42].

A similar effect leads to saturation of the PFWM waves and to suppression of ASE. At sufficiently high intensities of the ir and vuv waves generated by PFWM, these waves can lead to substantial pumping of the EF state by two-photon absorption. This leads to interference with the two-photon excitation by the uv pump laser and, as a consequence, the amplitude of this state and the polarization driving the PFWM process is reduced. The PFWM intensities saturate and the ASE radiation from the EF state is suppressed. This effect is called "two-photon cancellation effect" [20]. Saturation is expected as soon as we have $|M^s|^2 I_{uv}^2 \simeq |M^a| I_{ir} I_{vuv}$. The saturation power is therefore (with $I_{ir} = (\omega_{ir}/\omega_{vuv}) I_{vuv}$)

$$P_{vuvs} \simeq \sqrt{\omega_{vuv}/\omega_{ir}} |M^s/M^a| P_{uv} \ . \tag{17}$$

For the strongest transition observed at $\tilde{\nu}_{vuv} = 91\,540.5$ cm^{-1}, we obtain $P_{vuvs} \simeq 60$ kW and $P_{irs} \simeq 7$ kW (the additional s in the subscript stands for "saturation"). This exceeds the measured power (containing uncertainties in the pulse duration) by a factor of ~ 4 and demonstrates the possibility of generating vuv power of several 10 kW. It should be noticed that the saturation power depends only linearly on the uv pump power. It is, in addition, dependent on the spectral distance of the PFWM waves from B-state resonances so that with approaching the resonance the effect increases strongly and the saturation power decreases. This is probably the reason for the decrease of the ASE intensities with increasing gas admixture. The PFWM frequencies approach the resonances as an effect of the admixture so that the two-photon cancellation effect has a stronger influence. It is difficult to distinguish experientally between the different effects. The similarity of the phenomena observed in case of Na and the behavior in our experiment suggests, however, that interference effects in the polarization play a substantial role at higher H_2 pressures of several hundred mbar.

In the case of four-wave mixing experiments at smaller particle densities a limitation of the vuv intensity through interference effects does not seem to be likely. Interference effects would be efficient especially for vuv processes close to resonances and would therefore led to a flattening of the tuning profile. The agreement between the calculations in Fig. 5 (not including such effects) and the experimental result in Fig. 13 indicates that in this case saturation is not an important effect. The fact, however, that the calculated intensities are obviously by far too high demands that other limiting processes have to be considered. One possibility is the depletion of the ground state through processes other than FWM and PFWM. This suspicion is supported by the behavior represented in Fig. 9(b) concerning the PFWM ir wave with variation of the uv frequency. Neglecting the influence of the FWM, the high intensity of the pump radiation in connection with the lage cross section for two-photon absorption of $\sigma_0^{(2)} \simeq 1.74 \times 10^{-47}$ $cm^4 s$ [32] leads to an almost complete depletion of the ground-state population. H_2 molecules are either excited into higher vibrational levels by radiative processes (ASE, SEHRS in backward and forward directions), or are ionized or dissociated, respectively. At a pressure of 600 mbar the energy of the ir transitions in the backward direction at resonant $Q(1)$ excitation is found to be up to 100 μJ. This corresponds to 0.4×10^{15} photons emitted by 1×10^{15} particles in the $j = 1$ state in the focal range. Therefore, about 40% of the particles are accumulated in higher metastable vibrational ground state levels by the ASE radiation. We assume, in addition, that the very large absorption cross section connected with the EF state of $\sigma_{abs} \simeq 6.4 \times 10^{-18}$ cm^2 (including ionization and dissociation at $\lambda = 193$ nm [32]) causes a substantial reduction of the particle number available for radiation processes. Since the processes governing the depletion of the ground state and the various raditive processes as well as processes of recombination are highly dynamical, ground-state depletion is very difficult to predict quantitatively. If we make the simplifying assumption (in the frame of an order of magnitude estimate) that loss mechanisms prohibit molecules excited into the EF state to return back into the ground state—i.e., neglecting the influence of four-wave mixing and of recombination—the population of the ground state may be described by a simple rate equation. The quantity $[N(t) I_{uv}(t)]^2$ in Eq. (1) can then be replaced by a mean

value $(N_0 I_s)^2$ defined over the time interval from the onset of the laser pulse to the complete depletion of the ground state. For a bell-shaped laser pulse of maximum intensity 10^{11} W cm^{-2} and a duration of 1 ns (FWHM), we obtain for the depletion of the ground state from an initial density N_0 to 10% of this value after ~ 0.3 ns a value of $I_s \sim 10^{10}$ W cm^{-2} and the ratio $(I_s/I_{uv})^2 \sim 10^{-2}$. The maximum vuv intensity is now reduced to $\sim 10^9$ W cm^{-2} (as compared to 10^{11} W cm^{-2}) corresponding to a more realistic power of ~ 100 kW or a maximum conversion ir to vuv of $\sim 10\%$. Values of the power in the range of 10 to 100 kW seem realistic also in view of the considerably increased SRRS at pressures of several hundred mbar with irradiation of ir laser radiation as compared to the PFWM case. An assumed reduction of the ground-state population and connected with this the depletion of the intensity of the vuv wave could also represent an explanation for the two-photon cancellation effect obviously not effective at the small particle densities investigated.

The observation of HD in connection with four-wave mixing and SRRS in H_2/D_2 mixtures yields a clear indication that a high concentration of hydrogenic ions is present. The formation of HD occurs, as outlined in Sec. IV, along the reaction paths formulated there. HD has to be generated to a substantial degree not only in order to be relevant for phase matching in four-wave mixing, but also to guarantee a sufficient gain factor for stimulated resonant Raman scattering. We learn from the measurements in H_2 and D_2 that at least several 10 mbar of D_2 have to be present at the basic pressure of some 100-mbar H_2 in order to allow the observation of SRRS. A similar result is obtained from the calculations of the Raman gain coefficient outlined in Sec. II. The HD lines of Fig. 14(c) were measured at 160-mbar H_2 and 65-mbar D_2, respectively. If we assume that similar rules apply for scattering from HD, we are led to the conclusion that roughly 10% of H_2 and D_2 have reacted to HD. This is only possible if at least a corresponding amount of H_2 has been ionized or dissociated. It follows that ionization and dissociation are indeed important mechanisms leading to a depletion of the ground state. Another argument that supports the same conclusion is the observation that ir signals are only obtained from the leading peak of the uv pulse and not from the following portion that still contains $\sim \frac{2}{3}$ of the uv energy.

The existence of additional tunable lines in the spectral range of the longer-wavelength B-X transition is explained satisfactorily by stimulated resonant Raman scattering subsequent to the vuv wave generated by four-wave mixing. The origin of the tunability of the lines around the resonances $B(1)$-$X(7)$ is not readily explained. At hydrogen pressures of several hundred mbar, generation of a vuv wave by four-wave mixing directly on or in immediate proximity of the resonance does not seem possible. Following arguments given in Sec. II, we speculate that this effect is stimulated two-photon emission. In this case the $R(1)$ and $P(3)$ lines would correspond to $Q(1)$ and $S(1)$ transitions from $EF(6,1)$. The fact that in this experiment the uv laser was not spectrally at the two-photon resonance with the EF state and therefore could not generate directly a high population in the EF state seems to oppose this concept. With resonant $Q(1)$ excitation to $EF(6)$ the parallel ASE processes are too strong to allow the observation of a possible tunability induced by ir laser irradiation. The maximum of the tuning curve is found to be shifted by -1.5 cm^{-1} relative to the $R(1)$ resonance. In spite of the detuning of the two-photon excitation by -1.5 cm^{-1}, this indicates that in the maximum the frequency of the ir laser corresponds exactly to the resonance frequency of the transition $EF(6)$-$B(1)$ $P(2)$. Also in case of other choices of detuning of the uv laser (-2.4 and $+1.2$ cm^{-1}) the maximum intensity is always found exactly for the frequency of the ir laser corresponding to this resonance frequency (see Fig. 16). This suggests that this tuning effect is connected with fast particles in the Maxwell distribution that are resonantly two-photon excited. The Doppler shift of the ir transition of these particles amounts to a much lower value of only 0.2 cm^{-1} (this is clearly smaller than the laser linewidth) and therefore the ir resonance frequency appears to be unaffected. In the present case of $p = 300$ mbar, room temperature, and with a two-photon excitation at -1.5 cm^{-1}, approximately 2.5×10^{15} cm^{-3} can therefore be excited resonantly from $X(0,1)$ into $EF(6,1)$. Due to the ionization/dissociation from the EF state, one cannot expect an excited population of more than a few percent of the ground-state population. But this fraction clearly exceeds the threshold population density in the EF state for stimulated TPE as estimated in Sec. II (3×10^{13} cm^{-3}). Although this is a strong argument for the interpretation of the observed tunability as stimulated TPE, more detailed investigations seem to be necessary.

HD can be used as a medium for FWM alternatively to H_2. As shown in Ref. [44] two-photon excitation of HD with subsequent ASE emission in the ir and vuv is possible also in case of HD. In view of the resonance frequencies slightly shifted in HD, the possibility of generating tunable coherent radiation of high power in the vicinity of H_2 X-B resonance frequencies is opened. Such a source of radiation could, e.g., be useful for the detection of ground-state H_2. A possible limiting mechanism is the generation of molecular hyrogen in the focal region through the reaction of HD with hyrogenic ions. It is

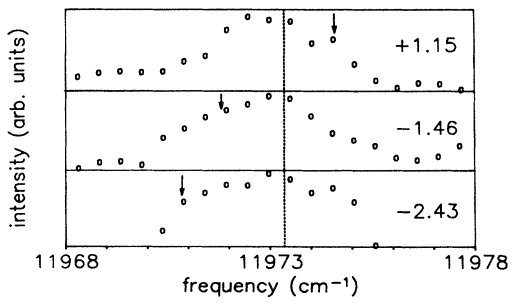

FIG. 16. Normalized intensities of the tuned $B(1)$-$X(7)$ $P(3)$ transition as a function of the ir laser frequency for various amounts of detuning of the uv two-photon excitation off the $Q(1)$ resonance (cm^{-1}).

not possible, however, to use D_2 alternatively to HD, since D_2 does not have two-photon resonances in the tuning range of ArF [45].

As can be seen from Table II, the transition $EF(6)$-$B(v)$ exhibits several transitions in the range 101–111 nm in the case of H_2, with large values of the transition moments $\tilde{M}$ in parallel to those investigated up to now. This is especially the case for $v_B=6$. This transition could allow very efficient generation of vuv radiation at the Lyman-β wavelength ($\lambda_\beta=102.6$ nm). The ir radiation necessary for FWM could be supplied by SRS in H_2. It is an open question, however, whether atomic hydrogen generated by photodissociation would limit the four-wave mixing at Lyman β.

Application of a pulsed H_2 nozzle should lead to higher vuv intensities through the connected reduction of absorption losses. It can be expected that the vuv radiation generated by PFWM could be extracted so that no additional ir laser irradiation would be necessary. We have shown in an earlier experiment that satellite lines, i.e., corresponding to PFWM, can be seen also with excitation by a simple oscillator-amplifier excimer laser system [9] so that the generation of short-wavelength vuv radiation (tunable by gas admixture) seems possible with a single laser system.

VI. CONCLUSIONS

We have shown that subsequent to two-photon excitation of H_2 several nonlinear optical processes take place. Besides ASE and SEHRS this is mainly PFWM and SRRS. These processes lead to the generation of several intense lines in the ir and vuv. vuv generation occurs along two paths: First, a vuv wave at ~ 109 nm is generated by PFWM. This wave generates SRRS, wich leads to Stokes waves at wavelengths around 150 nm. The corresponding frequencies can be tuned over small spectral intervals of the order of ~ 20 cm^{-1} by admixture of other gases (noble gases, N_2, D_2). The vuv intensities generated by PFWM reach ~ 16 kW.

Second, PFWM is replaced by FWM in the case of additional irradiation of intense ir laser light. In this case almost continuous tuning ranges of the vuv radiation over approximately 600 cm^{-1} can be realized. The tuning ranges are localized around the respective rovibronic resonances X-B. Exactly on resonance no FWM is possible. No measurements of the vuv power have been made so far. As discussed earlier, we assume that the power amounts to 10–100 kW. As in the case of PFWM, Stokes lines are also generated subsequent to FWM via SRRS. The tunability reaches 60 cm^{-1} in this case.

The susceptibilities governing the processes mentioned have been calculated. Very good agreement is observed between theoretical expectations and experimental observations. Furthermore, these calculations predict four-wave difference frequency mixing in hydrogen to be efficient in the range 101–111 nm. The calculated absolute values of the vuv intensities turn out to be by far too high. This is connected with the neglect of various limiting processes that have been discussed in connection with the experimental results. The mechanism of tunability of the vuv lines around the resonances $B(1)$-$X(7)$ still leaves some open questions. We speculate that this can be due to stimulated two-photon emission. Further clarification is needed.

ACKNOWLEDGMENTS

This work was supported by the Deutsche Forschungsgemeinschaft. Helpful discussions with Dr. C. R. Vidal are gratefully acknowledged.

[1] R. Hilbig, G. Hilber, and R. Wallenstein, Appl. Phys. B **41**, 225 (1986).
[2] P. R. Herman, P. E. La Rocque, R. H. Lipson, W. Jamroz, and B. P. Stoicheff, Can. J. Phys. **63**, 1581 (1985).
[3] R. T. Hudgson, P. P. Sorokin, and J. J. Wynne, Phys. Rev. Lett. **32**, 343 (1974).
[4] C. R. Vidal, in *Tunable Lasers,* edited by L. F. Mollenauer and J. C. White, Topics in Applied Physics, Vol. 59 (Springer-Verlag, Berlin, 1987).
[5] H. F. Döbele, M. Hörl, and M. Röwekamp, Appl. Phys. B **42**, 67 (1987).
[6] H. F. Döbele, M. Hörl, and M. Röwekamp, Appl. Phys. Lett. **49**, 925 (1986).
[7] H. Pummer, H. Egger, T. S. Luk, T. Srinivasan, and C. K. Rhodes, Phys. Rev. A **28**, 795 (1983).
[8] D. J. Kligler and C. K. Rhodes, Phys. Rev. Lett. **40**, 309 (1978).
[9] U. Czarnetzki, H. F. Döbele, and B. Rückle, Appl. Phys. B **48**, 37 (1989).
[10] U. Czarnetzki, U. Wojak, and H. F. Döbele, Phys. Rev. A **40**, 6120 (1989).
[11] U. Czarnetzki and H. F. Döbele, Phys. Rev. Lett. **64**, 2763 (1990).
[12] T. Srinivasan, H. Egger, H. Pummer, and C. K. Rhodes, IEEE J. Quantum Electron. **19**, 1270 (1983).
[13] D. L. Rousseau, J. M. Freidman, and P. F. Williams, *Raman Spectroscopy of Gases and Liquids,* edited by A. Weber (Springer-Verlag, Berlin, 1979).
[14] W. Hartig, Appl. Phys. **15**, 427 (1978).
[15] R. L. Byer and R. L. Herbst, *Nonlineaer Infrared Generation,* edited by Y.R. Shen (Springer-Verlag, Berlin, 1977).
[16] B. Nikolaus, D. Z. Zhang, and P. E. Toschek, Phys. Rev. Lett. **47**, 171 (1981).
[17] Y. R. Shen, *The Principles of Nonlinear Optics* (Wiley, New York, 1984).
[18] D. C. Hanna, M. A. Yuratich, and D. Cotter, *Nonlinear Optics of Free Atoms and Molecules* (Springer-Verlag, Berlin, 1979).
[19] A. Yariv, *Quantum Electronics* (Wiley, New York, 1975).
[20] R. K. Wunderlich, W. R. Garrett, R. C. Hart, M. A. Moore, and M. G. Payne, Phys. Rev. A **41**, 6345 (1990).
[21] Landolt-Börnstein, *Zahlenwerte und Funktionen, Band II* (Springer-Verlag, Berlin, 1962).
[22] E. Merzbacher, *Quantum Mechanics* (Wiley, New York,

1970).
[23] W. Fabian and B. R. Lewis, J. Quant. Spectrosc. Radiat. Transfer **14**, 523 (1973).
[24] J. Geiger and H. Schmoranzer, J. Molec. Spectrosc. **32**, 39 (1969).
[25] B. R. Lewis, J. Quant. Spectrosc. Radiat. Transfer **14**, 537 (1974).
[26] A. C. Allison and A. Dalgarno, J. Quant. Spectrosc. Radiat. Transfer **9**, 1543 (1969).
[27] A. C. Allison and A. Delgarno, Molec. Phys. **19**, 567 (1970).
[28] A. C. Allison and A. Delgarno, At. Data **1**, 289 (1970).
[29] R. J. Spindler, Jr., J. Quant. Spectrosc. Radiat. Transfer **9**, 597 (1969); **9**, 627 (1969).
[30] I. Dabrowski, Can. J. Phys. **62**, 1639 (1984).
[31] W. M. Huo and R. L. Jaffe, Chem. Phys. Lett. **101**, 463 (1983).
[32] J. D. Buck, D. C. Robie, A. P. Hickman, D. J. Bamford, and W. K. Bischel, Phys. Rev. A **39**, 3932 (1989).
[33] C. Leubner, H. Scheingraber, and C. R. Vidal, Opt. Commun. **36**, 205 (1981).
[34] H. Scheingraber and C. R. Vidal, IEEE J. Quantum Electron. **19**, 1747 (1983).
[35] P. Senn, P. Quadrelli, K. Dressler, and G. Herzberg, J. Chem. Phys. **83**, 962 (1985).
[36] J. Römelt, S. D. Peyerimhoff, and R. J. Buenker, Chem. Phys. **34**, 403 (1978); **41**, 133 (1979).
[37] D. J. Brink and D. Proch, Max-Planck-Institut für Quantenoptik, München, Report No. MPQ 65, 1982 (unpublished).
[38] D. Gerlich, *Symposium on Atomic and Surface Physics, Maria Alm/Salzburg, 1982,* edited by W. Lindinger, F. Howorka, T. D. Märk, and F. Egger (Universität Innsbruck, Innsbruck, 1984).
[39] Y. Ikezone, S. Matszoka, M. Takebe, and A. Viggiano, *Gas Phase Ion-Molecule Reaction Rate Constants Through 1986* (Ion Reaction Research Group, Maruzen Comp. Ltd., Tokyo, 1987).
[40] N. G. Adams and D. Smith, *Reactions of Small Transient Species,* edited by A. Fontijn and M. A. A. Clyne (Academic, London, 1983).
[41] E. E. Marinero, C. T. Rettner, and R. N. Zare, J. Chem. Phys. **80**, 4142 (1984).
[42] M. A. Moore, W. R. Garrett, and M. G. Payne, Opt. Commun. **68**, 310 (1988).
[43] R. W. Boyd, M. S. Malcuit, D. J. Gauthier, and K. Rzążewski, Phys. Rev. A **35**, 1648 (1987).
[44] T. S. Luk, H. Egger, W. Müller, H. Pummer, and C. K. Rhodes, in *Ultrafast Phenomena IV,* edited by H. Austen and K. B. Eisenthal (Springer-Verlag, Berlin, 1984).
[45] K. Dressler and L. Wolniewicz, J. Chem. Phys. **82**, 3292 (1985).
[46] *Spectroscopic Data, Volume 2, Homonuclear Diatomic Molecules,* edited by S. N. Suchard and J. E. Melzer (IFI/Plenum Data, New York, 1976).
[47] H. Schmoranzer (private communication).